Sliding-mode control of single input multiple output DC-DC converter

Article *in* Review of Scientific Instruments · October 2016

DOI: 10.1063/1.4963694

CITATION
1

READS
336

4 authors, including:

Libo Zhang
Chinese Academy of Sciences
59 PUBLICATIONS **165** CITATIONS
SEE PROFILE

Tiejian Luo
Chinese Academy of Sciences
105 PUBLICATIONS **350** CITATIONS
SEE PROFILE

AIP | Review of Scientific Instruments

Sliding-mode control of single input multiple output DC-DC converter

Libo Zhang, Yihan Sun, Tiejian Luo, and Qiyang Wan

Citation: Review of Scientific Instruments **87**, 104703 (2016); doi: 10.1063/1.4963694
View online: http://dx.doi.org/10.1063/1.4963694
View Table of Contents: http://scitation.aip.org/content/aip/journal/rsi/87/10?ver=pdfcov
Published by the AIP Publishing

Sliding-mode control of single input multiple output DC-DC converter

Libo Zhang,[a] Yihan Sun, Tiejian Luo, and Qiyang Wan
University of Chinese Academy of Sciences (UCAS), Beijing 100049, China

(Received 13 April 2016; accepted 13 September 2016; published online 4 October 2016)

Various voltage levels are required in the vehicle mounted power system. A conventional solution is to utilize an independent multiple output DC-DC converter whose cost is high and control scheme is complicated. In this paper, we design a novel SIMO DC-DC converter with sliding mode controller. The proposed converter can boost the voltage of a low-voltage input power source to a controllable high-voltage DC bus and middle-voltage output terminals, which endow the converter with characteristics of simple structure, low cost, and convenient control. In addition, the sliding mode control (SMC) technique applied in our converter can enhance the performances of a certain SIMO DC-DC converter topology. The high-voltage DC bus can be regarded as the main power source to the high-voltage facility of the vehicle mounted power system, and the middle-voltage output terminals can supply power to the low-voltage equipment on an automobile. In the respect of control algorithm, it is the first time to propose the SMC-PID (Proportion Integration Differentiation) control algorithm, in which the SMC algorithm is utilized and the PID control is attended to the conventional SMC algorithm. The PID control increases the dynamic ability of the SMC algorithm by establishing the corresponding SMC surface and introducing the attached integral of voltage error, which endow the sliding-control system with excellent dynamic performance. At last, we established the MATLAB/SIMULINK simulation model, tested performance of the system, and built the hardware prototype based on Digital Signal Processor (DSP). Results show that the sliding mode control is able to track a required trajectory, which has robustness against the uncertainties and disturbances. *Published by AIP Publishing.* [http://dx.doi.org/10.1063/1.4963694]

I. INTRODUCTION

With the accelerated development of urbanization and sustained growth of vehicle population, the research on the vehicle mounted power system has been attracting more and more attention.[1–3] The power source makes a big difference to the performance of the whole vehicle, which becomes the most significant component in an automobile. There are various kinds of vehicle equipment, including automotive lighting, scavenging pump, rain wipers, and air conditioning system. Because a certain kind of equipment works on its rated power different from others', it may need a certain appropriate input voltage, which results in diverse demands of voltage by all kinds of equipment on a 14 V-output vehicle mounted power system. Conventional solution is supplying power to different equipment by utilizing multiple DC-DC converters with various output voltages. But the cost of this solution is high, the space these converters occupied is inessential actually, and the interference between converters cannot be avoided completely as well. It's necessary for us to design a Single Input Multiple Output (SIMO) converter of high integration.

In general, various SIMO DC–DC converters with different voltage outputs are combined to meet the demand of specific voltage levels. Obviously, the more the converter's system controller simplifies, the less its corresponding cost is.[4–6] A number of researches on SIMO switching converters which can simultaneously generate buck and boost output voltage have been reported over the last decade.[7–10] Ref. 7 uses the peak current control method and state machine to regulate output voltage. Ref. 8 proposes the charge control method and divides one period to regulate the multiple output voltages. Due to the high freewheeling current level, they perform the low power conversion efficiency in light-load condition. The works in Refs. 9–12 introduce time multiplexing techniques, which we can use to regulate the multiple output voltages and reduce cross-regulation. According to the opinion in Ref. 13, freewheeling current can be monitored with the inductor current control method for dual boost output voltages.

Patra *et al.*[21] have designed a SIMO DC-DC converter which can both boost voltage and generate buck, but for each output it demands three switches. It cannot be applied to the situation in need of the high output voltage, and its hard switching operation results in its low efficiency in power conversion. Chen *et al.*[22] have realized zero-current switching for the lagging leg with their multiple output DC-DC converter. Compared with Patra's converter, this converter solves the problem of power losses, at the expense of more complexity and higher cost. Nami *et al.*[23] have presented a multiple output DC-DC converter, which can output a series of low and high voltages. However, there are still over two switches used for each output, which leads to the complexity of its control scheme. Another disadvantage is that it cannot independently provide power for a certain load. A series of SIMO converters in Ref. 24 can output multiple voltages through multiple secondary windings with high frequency AC, while regulating each output is difficult because of the magnetic coupling. A SIMO DC-DC converter with a less number of switches was

[a]Author to whom correspondence should be addressed. Electronic mail: zsmj@hotmail.com

proposed in Ref. 25, which simultaneously generates buck and boost outputs. It utilizes a hysteresis mode to increase stability when unbalanced output loads occur. There are a few particular blocks required such as a power comparator and a delta-voltage generator circuit while implementing the hysteresis mode. Unfortunately, when the buck output is charged, the current goes through the resistive freewheeling switch rather than the inductor, which also reduces the power conversion efficiency.

In our research, a SIMO-DC–DC converter with a coupled inductor is designed and implemented. The proposed converter achieves the characteristics of efficient power conversion, electric isolation, high step-up/step-down ratios, and various output voltages with different levels. In the proposed SIMO-DCDC converter, the techniques of voltage clamping are adopted to reduce the switching and conduction losses via the utilization of low-voltage-rated power switches. Additionally, it also solves the problems of the stray inductance energy and reverse-recovery currents within diodes in the conventional boost converters. Compared with these conventional converters, there is a significant improvement by using coupled inductor topology. Unfortunately, it is complicated to design and control it to guarantee the dynamic robustness for extended operating conditions. The work in Ref. 26 distributes the four output voltages into two parts: the first three output voltages controlled by comparators, and the last one controlled by an error amplifier. But this structure and control method will restrict the flexibility of the buck and boost output voltages. As an alternative, the sliding mode control is a better choice because of its attractive performance for controlling power exchanges by appropriate switching devices.[14,15] Sliding mode control is a powerful and excellently robust nonlinear control method. Sliding mode control is a nonlinear control method with high robustness against uncertain factors, load perturbation, and dynamic variations.[27] Sliding mode controller is suitable for our application because it is much easier to implement compared with other nonlinear controllers. In general, it is most appropriate to utilize sliding mode control in our DC-DC controller as the most powerful robust control strategies. In some papers, SMC has been utilized to control the DC-DC converters and some researches have indicated that SMC can ensure DC-DC converter to maintain stability and splendid dynamic performance with small range variable loads.[16,17] SMC also has advantages such as simplicity, easy implementation, and strong robustness by operating at switching frequency. A sliding mode control of hybrid DC power source applied to hybrid electric vehicles was proposed in Ref. 18. In Ref. 19, Wang introduced a TSM control method for output voltage tracking of a buck converter by using fuzzy logic to guarantee its robustness. Some researchers proposed an adaptive method to obtain the input voltage and the load resistance,[28] so as to calculate the reference current. Nevertheless, it is complicated and indirect to calculate it and unclear on how to obtain the expected performance. Of course, it is not really a sliding mode controller completely, and it is difficult to decide the control parameters.

According to the analyses above, the single input multiple output converter we design overcomes the disadvantages such as complicated structure, high scheme cost, low integration in conventional multiple output DC-DC converters. In particular, we utilize a coupled inductor in our SIMO converter coping with the complex structure in conventional SIMO converters. The proposed converter has characters of efficient power conversion, excellent electric isolation, high step-up/step-down ratios, and multiple outputs of various voltage levels. We adopt the voltage clamping in the SIMO converter so as to keep a high conversion efficiency in use of low-voltage-rated power switches with small RDS(on). As a result, this scheme also solves the problem of the stray inductance energy and reverse-recovery currents in diodes, which reduces the power conversion efficiency. Then the adjustment of middle-voltage output terminals in our converter is controlled by the auxiliary inductors in the scheme. In order to improve the performance of the SIMO converter, the SMC-PID control algorithm is presented, which is implemented by the SMC-PID controller. The SMC-PID controller is a normal sliding-mode controller with a PID control module, in which the integral of voltage error is utilized to decline the control error of the sliding-mode control system.

This paper is organized as follows. Section II describes design and analyses of the converter. Section III explores the modeling and analysis of sliding mode controller. In Section IV, the experimental results show the performance of the proposed sliding-mode control of the SIMO DC-DC converter. Finally, the conclusion is made in Section VI.

II. CONVERTER DESIGN AND ANALYSES

In order to generate multiple outputs, this paper uses two different voltage levels from a single input source. The configuration of the proposed high-efficiency SIMO converter is represented in Fig. 1 which shows that the system circuit is divided into four parts, including the input voltage circuit, low voltage output circuit, high voltage output circuit, and clamp circuit. The major symbol representations are summarized as follows. V_{in}, L_p, S_1 constitute the input voltage circuit. The clamped circuit consists of D_1, C_1, S_2. The high voltage output circuit includes L_s, C_2, D_3, D_4, C_{01}, R_{01}, while the low voltage output circuit contains L_{aux}, D_2, C_{02}, D_3, R_{02}. $V_{01}(I_{01})$ and $V_{02}(I_{02})$, respectively, denote the voltages (currents) of the high voltage output circuit and low voltage output circuit; V_{in} and I_{in} are the input voltage and current in the input voltage

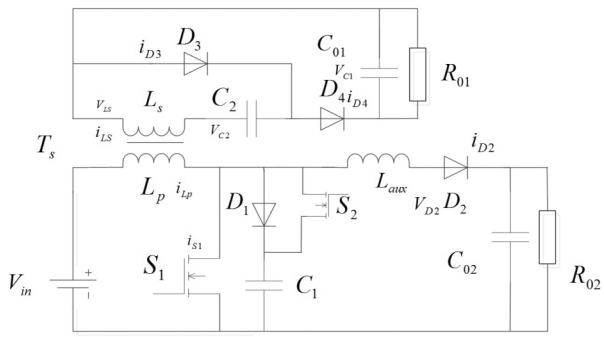

FIG. 1. System configuration of single-input multiple-output (SIMO) configuration.

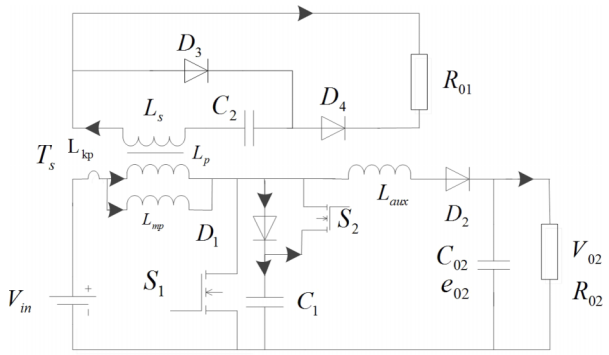

FIG. 2. Equivalent circuit of the SIMO converter.

circuit. In addition, R_{01}, R_{02} are the equivalent loads in the high voltage output circuit and low voltage output circuit. L_p and L_s represent individual inductors in the primary and secondary sides of the coupled inductor (T_s) respectively, where the primary side is connected to the input voltage circuit; L_{aux} is the auxiliary inductor in the low voltage output circuit.

In our research, the following assumptions are made to simplify the converter analyses: (1) The switches including their body diodes are assumed as ideal switching elements. (2) The conduction voltage drops of the switches and diodes are neglected. The corresponding equivalent circuit provided in Fig. 2 defines the voltage polarities and current directions. The coupled inductor in Fig. 1 can be modeled as an ideal transformer including the magnetizing inductor L_{mp} and the leakage inductor L_{kp} in Fig. 2. The turn ratio N and coupling coefficient k of this ideal transformer are defined as

$$N = N_2/N_1, \tag{1}$$

$$k_p = L_{mp}/\left(L_{mp} + L_{kp}\right) = L_{mp}/L_p, \tag{2}$$

where N_1 and N_2 are the winding turns in the primary and secondary sides of the coupled inductor T_s. Then there are another two assumptions made to simplify the converter analyses: (1) The main switch including its body diode is assumed to be an ideal switching element and (2) the conduction voltage drops of the switch and diodes are neglected. The characteristic waveforms are depicted in Fig. 3, and the topological modes in one switching cycle are illustrated in Fig. 4.

Mode 1 (t_0-t_1) [see Fig. 4(a)]: In this mode, the switch S_1 is turned ON, and the switch S_2 is turned OFF for a span. Because the magnetizing inductor L_{mp} is charged by the input power source V_{in}, the magnetizing current i_{Lmp} increases gradually in an approximately linear trajectory. The secondary voltage V_{LS} charges the low voltage output circuit capacitor C_2 through the low voltage output circuit diode D_3. When the auxiliary inductor L_{aux} releases its stored energy completely, the diode D_1 turns OFF, which marks the end of this mode.

Mode 2 (t_1-t_2) [see Fig. 4(b)]: In this mode, the switch S_1 is persistently turned ON, the switch S_2 is turned OFF. The secondary voltage V_{LS} charges the low voltage output circuit capacitor C_2 through the low voltage output circuit diode D_3. According to Kirchhoff's voltage law, the input power source V_{in} can be represented as

$$V_{in} = V_{Lp} + V_{Lkp} = V_{Lp}V_{Lp}\left(1 - k_p\right)/k_p = V_{Lp}/k_p. \tag{3}$$

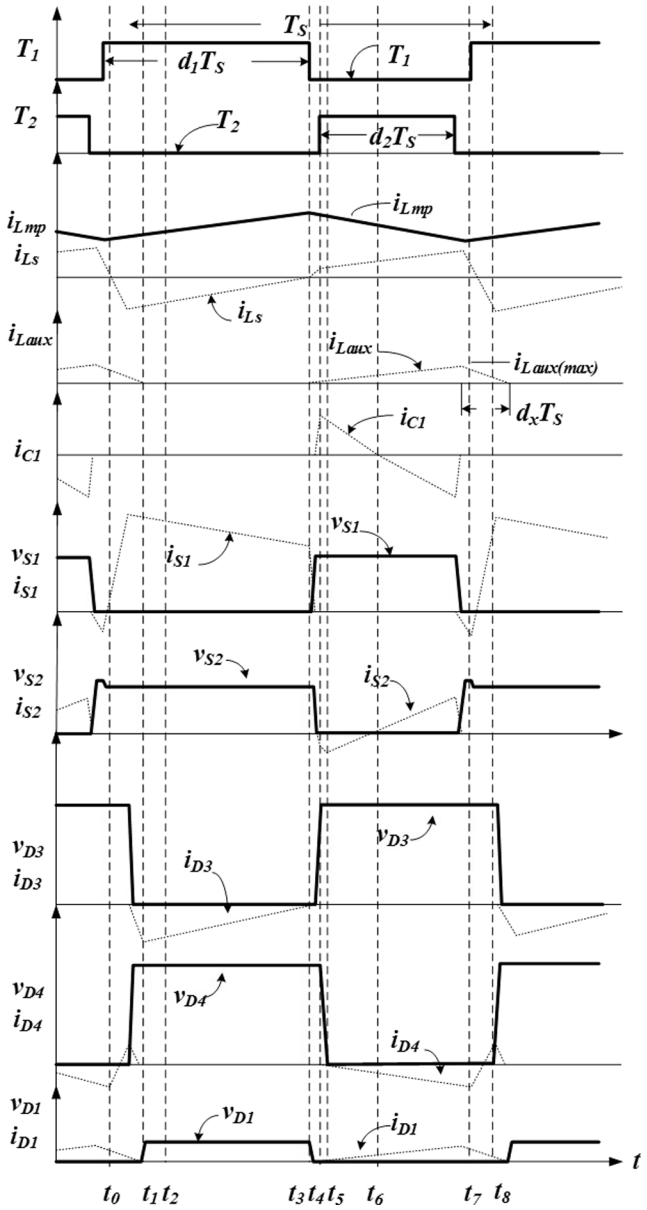

FIG. 3. Characteristic waveforms of the SIMO converter.

From Eq. (3), the voltage V_{C2}, which is equal to the voltage V_{LS}, can be computed as

$$V_{C2} = V_{LS} = NV_{LP} = k_pNV_{in}. \tag{4}$$

Mode 3 (t_2-t_3) [see Fig. 4(c)]: At time $t = t_2$, the switch S_1 and low voltage output circuit diode D_3 are turned OFF. After that, the diode of D_3 conducts to carry the secondary current i_{LS}, because the stored energy in the coupled inductor T_S needs to release. The primary current i_{Lp} charges the parasitic capacitor of the switch S_1, and partial energy of the primary winding L_p is transmitted to the auxiliary inductor L_{aux}. When the secondary inductor L_s releases its stored energy completely, and the secondary current i_{LS} gradually decays to zero, this mode ends.

Mode 4 (t_3-t_4) [see Fig. 4(d)]: At time $t = t_3$, the secondary current i_{LS} is induced in reverse. In this mode, the secondary winding L_s of the coupled inductor and the capacitor C_2 connect in series to release the energy into the high voltage

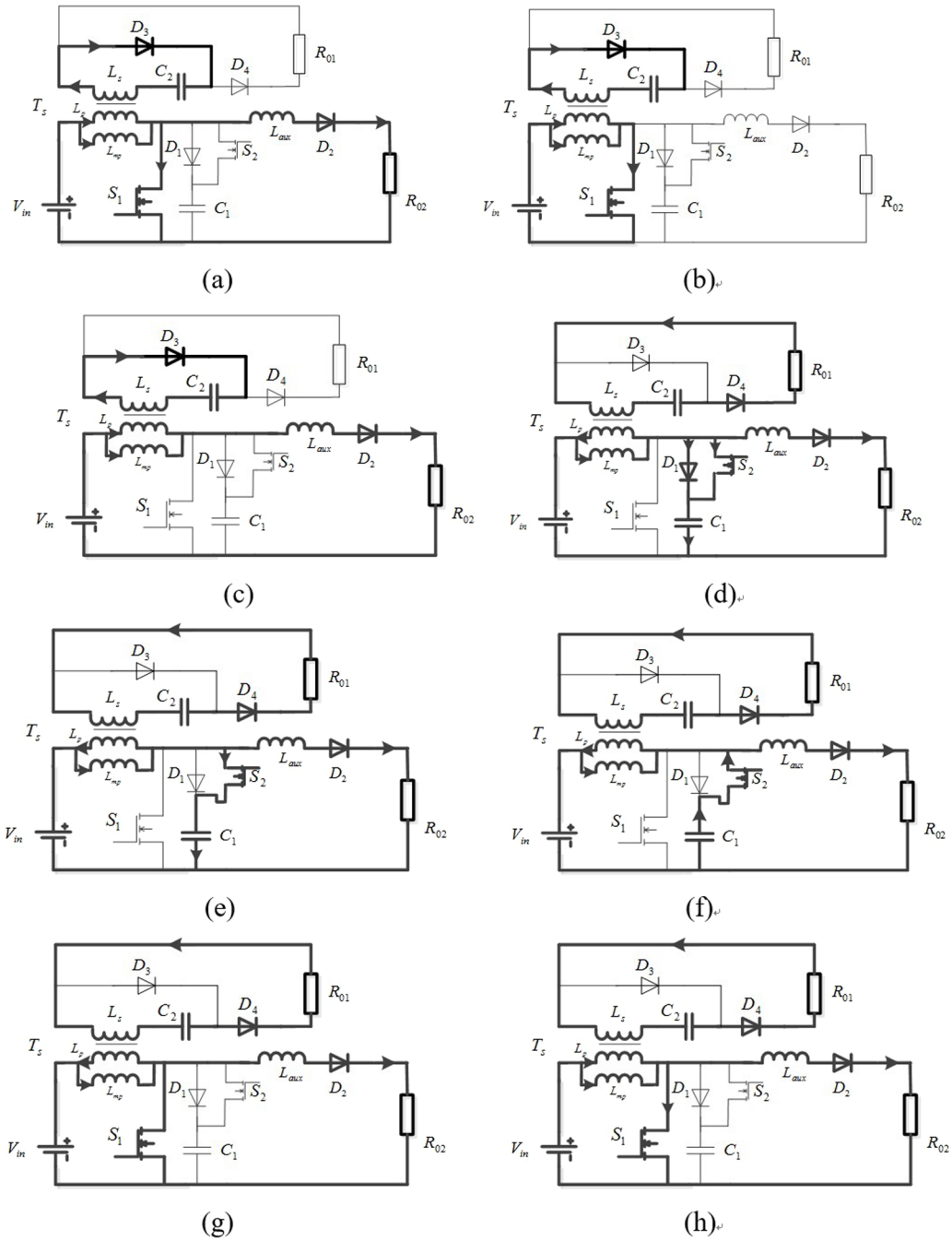

FIG. 4. Topological modes at step-up state: (a) mode 1 [t_0-t_1]; (b) mode 2 [t_1-t_2]; (c) mode 3 [t_2-t_3]; (d) mode 4 [t_3-t_4]; (e) mode 5 [t_4-t_5]; (f) mode 6 [t_5-t_6]; (g) mode 7 [t_6-t_7]; (h) mode 8 [t_7-t_8].

output circuit through the diode D_4. Meanwhile the clamped diode D_3 and the switch S_2 conduct to transmit the energy of the primary-side leakage inductor L_{kp} into the clamped capacitor C_1. According to Kirchhoff's voltage law, the voltages V_{Lp} and L_{LS} can be represented as:

$$V_{Lp} = k_p\,(V_{in} - V_{C1})\,, \tag{5}$$

$$V_{LS} = NV_{Lp}. \tag{6}$$

Mode 5 (t_4-t_5) [see Fig. 4(e)]: At time $t = t_4$, the clamped switch S_2 and the diode D_4 are turned ON. The secondary winding L_{aux} of the coupled inductor and the capacitor C_2 connect in series to continuously release the energy from the energy of the magnetizing inductor into the high voltage output circuit through the diode D_4. Then, the clamped capacitor current i_{CL} drops to zero, and this mode ends.

Mode 6 (t_5-t_6) [see Fig. 4(f)]: At time $t = t_5$, the current i_{CL} returns to zero because the leakage inductor L_{kp} releases its energy completely. At the same time, the clamped capacitor C_1 starts to release its stored energy into the auxiliary inductor through the clamped switch S_2.

Mode 7 (t_6-t_7) [see Fig. 4(g)]: At time $t = t_6$, the body diode of the switch S_1 conducts to carry the current i_{Lkp} because the primary winding of the coupled inductor T_S releases its stored energy persistently. At the moment, the auxiliary inductor L_{aux} starts to release its stored energy for the source

V_{02} through the diode D_1 via the floating charge type. When the primary winding of the coupled inductor T_S releases its leakage energy completely, the current i_{Lkp} drops to zero, and this mode terminates.

Mode 8 (t_7-t_8) [see Fig. 4(h)]: At time t = t_7, the low-voltage switch S_1 is turned ON. During the interval, the secondary current i_{LS} gradually decays to zero, and reverses in the later stage of this mode. When the diode D_4 turns OFF, the diode D_3 turns ON to carry the secondary current i_{LS}. Then, it begins the next switching cycle and repeats the operation from mode 1.

III. CONTROL ALGORITHM ANALYSIS

In order to implement the SIMO-DC–DC converter, the first step is the choice of the state variables. According to the suggestions in Ref. 20, since the magnetic flux is not directly measurable, the current i_m defined as follows will be employed:

$$i_m = \begin{cases} i_{Lp} & t \in [0, T_{ON}] \\ i_{Lp}(1+N) & t \in [T_{ON}, T] \end{cases}, \tag{7}$$

where $T = T_{ON} + T_{OFF}$ is the switching time period, N is the ratio of the secondary winding turns to the primary winding ones, and i_{LP} is the primary winding current. As shown in Fig. 2, the corresponding equivalent dynamic equation is given as

$$u = \begin{cases} R_{02} + L_p(1+N)\dfrac{di_m}{dt} = V_{in} - (1-u)\,e_{02} \\ C_{02}\dfrac{dV_{in}}{dt} = \dfrac{(1-u)}{1+N} i_m - i_{Laux} \end{cases}, \tag{8}$$

where $u \in (0, 1)$. More specifically, $u = 1$ when S_1 is ON and S_2 is OFF; $u = 0$ when S_1 is OFF and S_2 is ON. The vector x of state-variables error is defined as:

$$X = [x_1, x_2]' = \left[i_m - I_m^{ref}, e_{02} - V_{02}^{ref}\right]'. \tag{9}$$

The standard modeling can be deduced as the following:

$$\dot{X} = Ax + Bu + Az + D. \tag{10}$$

Among

$$z = \left[I_m^{ref}, V_{02}^{ref}\right], \tag{11}$$

$$A = \begin{bmatrix} -\dfrac{R_{02}}{L_1(1+N)} & -\dfrac{1}{L_1(1+N)} \\ \dfrac{1}{C_{02}(1+\mathrm{N})} & 0 \end{bmatrix}, \tag{12}$$

$$B = \begin{bmatrix} \dfrac{e_{02}}{L_1(1+N)} \\ -\dfrac{i_m}{C(1+N)} \end{bmatrix}, \tag{13}$$

$$D = \begin{bmatrix} \dfrac{V_{in}}{L_1(1+N)} \\ -\dfrac{i_{in}}{C(1+N)} \end{bmatrix}, \tag{14}$$

$$I_m^{ref} = \frac{1+N}{1-d^{ref}} I_{02}^{ref}. \tag{15}$$

The choice of the ratio N is affected at no-load operating condition by imposing the lowest admissible duty ratio. According to the variable structure system theory, a sliding surface must be chosen within the state variables space, where control functions are discontinuous. As a consequence of the feedback control, the system structure alters when the state variables cross the mentioned surfaces. In general, two different dynamic conditions can be distinguished:

- reaching dynamics, which is a fast dynamic, forcing the state variables of the system towards the sliding surfaces;
- sliding dynamics is a slower dynamic condition, where the state variables "slid" towards the origin of the state space and remain in the sliding subspace.

The following sliding surface is chosen:

$$ref = k_1 x_1 + k_2 x_2, \tag{16}$$

where k_1 and k_2 are the control parameters, *ref* is a reference input. The system may generate the steady state error once the operating points change, so the sliding mode surface is modified to

$$S(x) = k_1 x_1 + k_2 x_2 + k_3 \int_0^t (x_2 - v_{ref})\, dt = 0, \tag{17}$$

where V_{ref} is the referenced input voltage.

By assuming the ideal hypothesis of infinite commutation frequency of electronic switches, the control law is set as

$$u = \begin{cases} 1 & S(x) < 0 \\ 0 & S(x) > 0 \end{cases}. \tag{18}$$

The hysteresis band can be easily derived once the maximum switching frequency has been fixed. More specifically, it is evaluated in correspondence to the no-load operating condition involving the maximum switching frequency. We assume that the error variables are conveniently smaller than the corresponding references and neglect the loss parameter. The following inequality can be derived for guaranteeing the existence of sliding mode:

$$k_1 > k_2 \frac{L_p}{C_{02}} \frac{I_{02}^{ref}}{V_{in}}. \tag{19}$$

Once the maximum value of the reference current and the minimum value of supercapacitor discharge voltage have been estimated, k_1 and k_2 can be selected properly.

IV. SIMULATION ANALYSIS

According to the design rules of the power system mounted on electric vehicle, we adopt the 14 V vehicle power system. The power system supplies air conditioning compressor, cooling fan, each LED lamp, and so on. Because of differences among their voltage levels, the design of the SIMO converter selects 48 V and 24 V as outputs in the research. With the above analysis, the main parameters in the design of the SIMO converter are as follows:

The input voltage: 12-16 V.

The rated input voltage: V_{in} = 14 V.

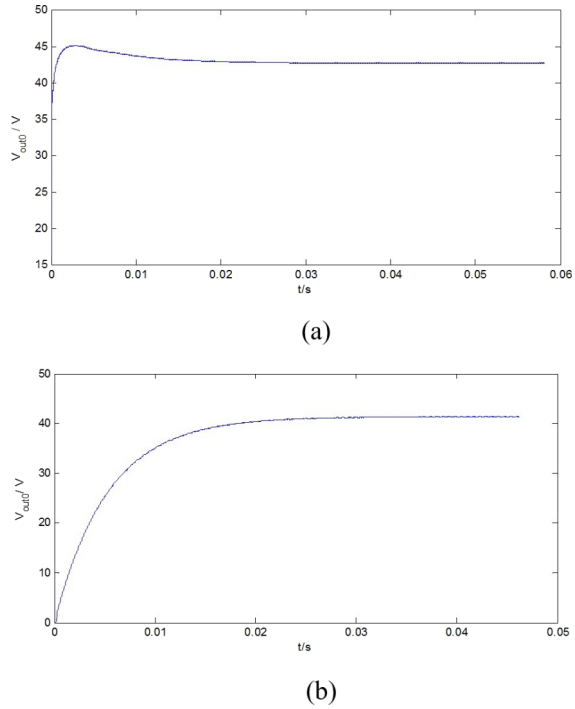

FIG. 5. The output voltages of conventional control algorithm: (a) feedback algorithm; (b) SMC algorithm.

The rated output voltage: $V_{01} = 48$ V, $V_{02} = 24$ V.

The series resonant frequency: $f_s = 100$ KHz.

Based on the analysis of the circuits and the algorithm of the sliding mode control, we simulate the SIMO DC–DC converter on MATLAB/SIMULINK. With the requirements of design and the data comparison among the actual simulations, the following parameters of the circuit are determined: $L_p = 75$ μH, $L_{aux} = 20$ μH, $L_S = 10$ μH, $C_{02} = 50$ μF, $C_1 = 200$ μF, $C_2 = 10$ μF. According to the actual simulation tests, the corresponding PID parameters are obtained.

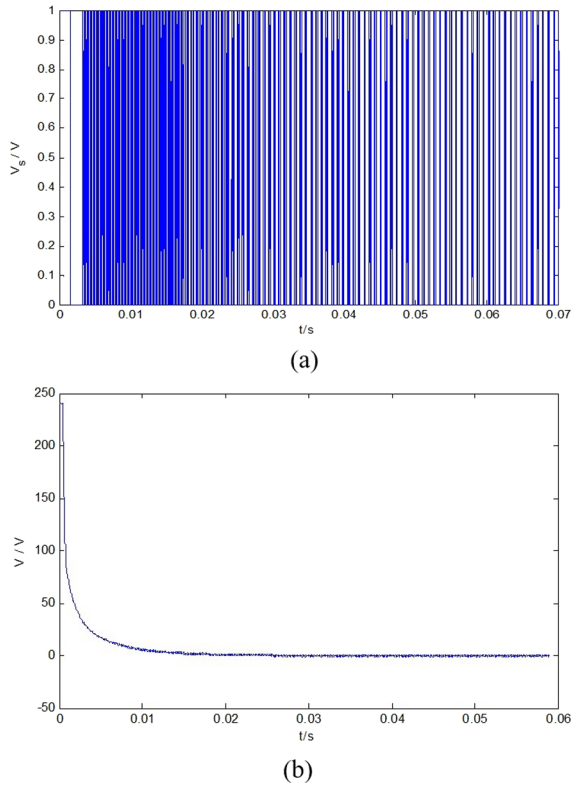

FIG. 7. (a) Output waveform of sliding-mode controller; (b) output waveform of PID.

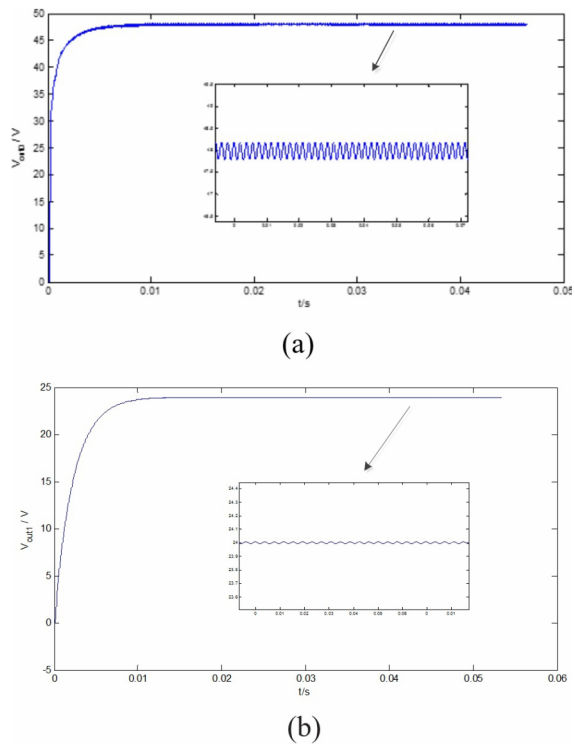

FIG. 6. Experimental output voltages of SIMO converter: (a) high-voltage output; (b) low-voltage output.

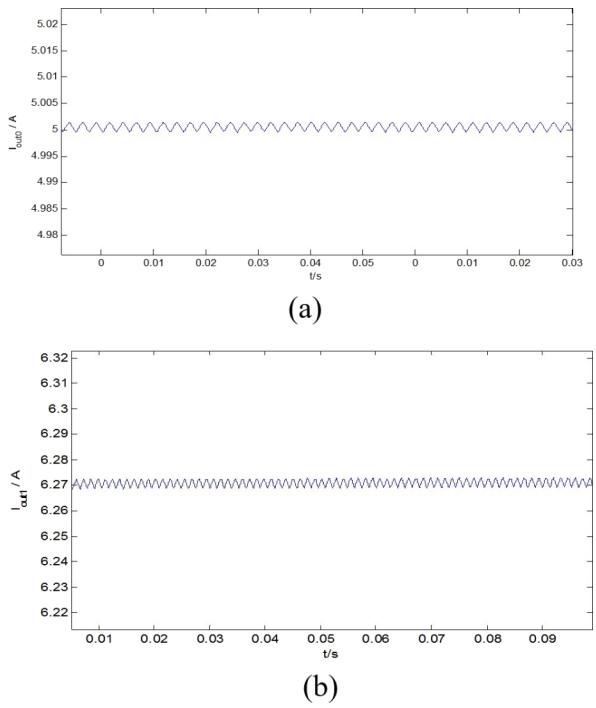

FIG. 8. Experimental output current of SIMO converter: (a) current waveform of high-voltage output with rated power; (b) current waveform of low-voltage output with rated power.

The main purpose of designing the SIMO converter is to obtain multiple outputs from single input, and maintain the output voltages stable by taking advantage of the SMC-PID control algorithm.

In order to analyze the performance of the SIMO converter further, we introduce the conventional feedback control algorithm and conventional SMC control algorithm, and the simulation results are shown in Fig. 5. The results indicate that the overshoot of the conventional algorithm in Fig. 5(a) is much larger. And based on the same timeline, the time used to reach the stable state in Fig. 6(a) is much less than that in Fig. 5(b), which demonstrates that PID-SMC control algorithm has the better performance of dynamic response than the conventional algorithm.

The waveforms of the output voltage V_{01} and V_{02} are, respectively, illustrated in Fig. 6. The high voltage V_{01} and the low voltage V_{02} can rapidly reach a stable state. The amplified voltage waveforms show the rated values of voltage ripple are approximately 1% both in the 48 V high output voltage and 24 V low output voltage.

The output of PID during the stabilizing process of the SIMO converter is presented in Fig. 7. The output of PID is large when there is a huge difference between the expected voltage and the actual voltage in the beginning, while it slumps in no time under the adjustment of the feedback system. This output keeps stable of zero when the load remains steady. Fig. 7(a) shows the output waveform of sliding-mode controller, that is, the driving waveform on main switch S_1 and S_2. The output tends to be steady when the load does not change after the fluctuation during startup state.

By adjusting the output load, the SIMO converter can work at the maximum power output. The corresponding currents of the two outputs are measured and shown in Fig. 8. Fig. 8(a) indicates the current waveform of the high voltage output at the maximum power (P_{out01} = 240 W) and the current keeps stable at about 5 A. Fig. 8(b) shows the current waveform of the low voltage output at the maximum power (P_{out02} = 150 W) and the current keeps stable at about 6.27 A.

Fig. 9 shows the waveform of the output voltage (a), output current (b), and sliding mode control signal (c) when the load resistance changes from 12 Ω to 8 Ω. As the simulation results indicate, the oscillating behavior of the output voltage during transient and load resistance change is inhibited. It takes less time to start the sliding mode as expected.

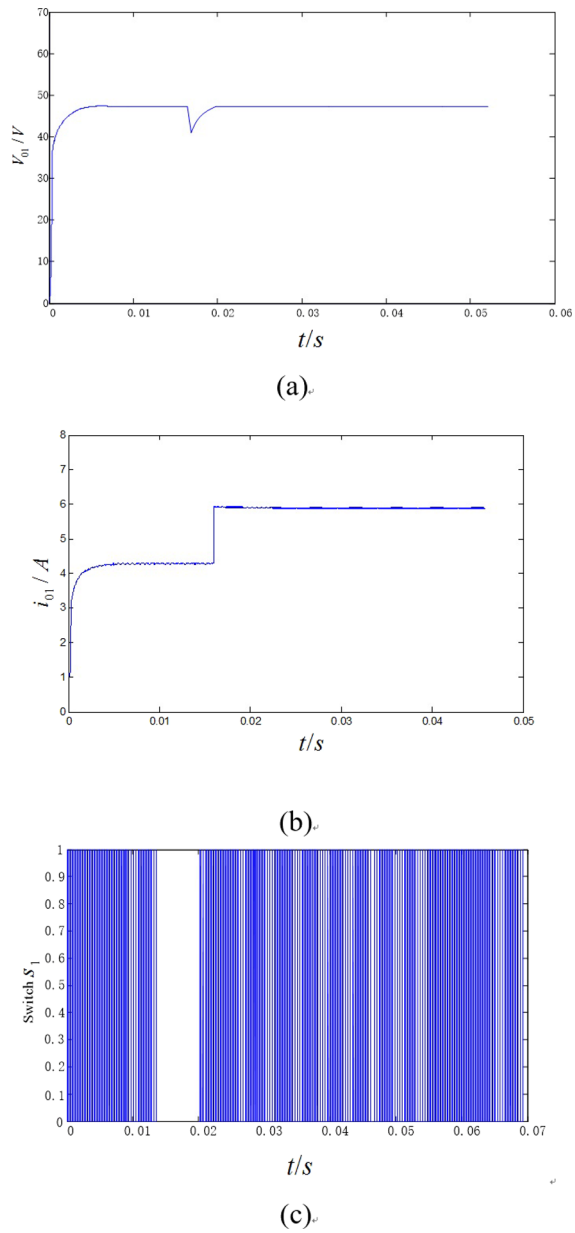

FIG. 9. Load resistance switching from 12 Ω to 8 Ω: (a) high output voltage; (b) output current; (c) switch control.

V. EXPERIMENTAL RESULT

In this research, the sliding mode control is used to handle the situation that the output voltage varies with load variation, and a digital-signal-processor TMS320F2812 manufactured by Texas Instruments is adopted to achieve the goal of feedback control. According to the principle of SIMO design, the high power LED group is connected into the high voltage output circuit as the load, and the various resistances are used in the low-voltage side as the load respectively, to simulate the lights, air conditioners, and other equipment of electric cars.

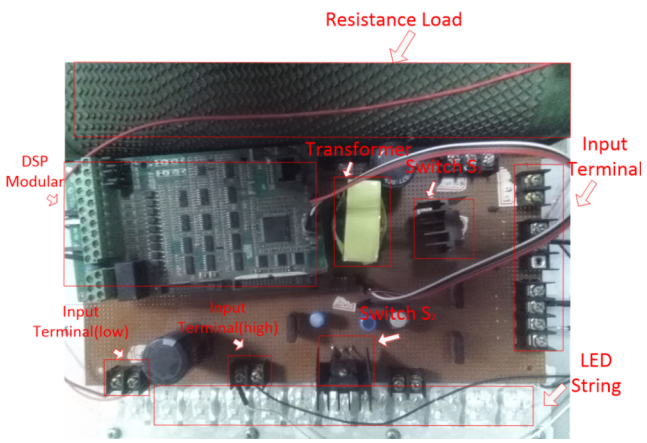

FIG. 10. Practical photograph of the entire experimental setup.

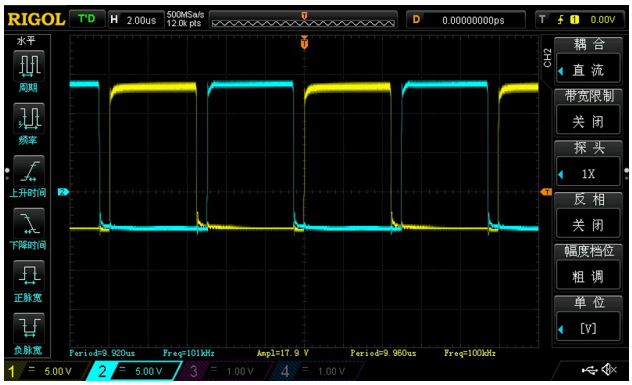

FIG. 11. SIMO driving voltage waveform of switch and (yellow line: the waveform of S1; blue line: the waveform of S2).

The practical photograph of the entire experimental setup is depicted in Fig. 10.

In our fixed frequency PID-SMC control algorithm, the circuit switching frequency is 100 KHz while the duty cycle varies according to the input. The driving waveforms of switch S_1 and S_2 are shown in Fig. 11. In Fig. 11, the yellow line represents the waveform of S1, while the blue one shows that of S2, which indicate that there is a certain dead time between S1 and S2. There is a dead time between S_1 and S_2 waveforms, which meets the design requirements of the circuit.

The experimental data are measured with resistive load and LED load. The waveforms of the output voltages are shown in Fig. 12. In Fig. 12(a), the high output voltage keeps stable at 48 V and the LED string works regularly. The low output voltage waveform is shown in Fig. 12(b), where the voltage ripple rated value is less than 3%.

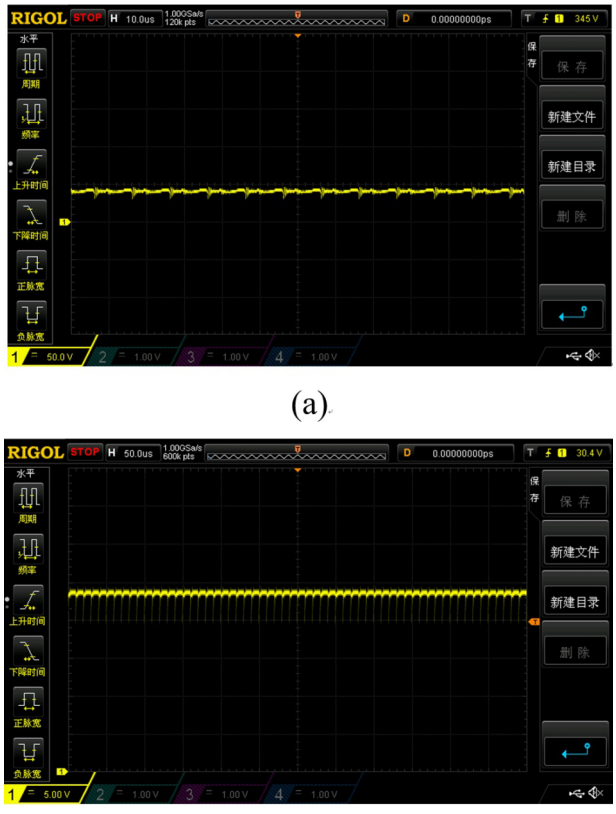

(a)

(b)

FIG. 12. Prototype output voltage waveform: (a) high output voltage; (b) low output voltage.

VI. CONCLUSIONS

In this study, an efficient SIMO DC–DC converter is designed successfully, and this coupled-inductor-based converter has been applied well to a single-input power source with two output terminals, which consist of a high voltage output circuit and a low voltage output circuit. Meanwhile, this paper utilizes the SMC-PID to control the DC–DC converter and the experimental results have indicated that SMC-PID can guarantee the DC-DC converter to work stably and show excellent dynamic performance with small range variable loads. The feasibility of this solution is validated by a MATLAB/SIMULINK simulation. A prototype with the load of LED and pure resistance is built based on the theoretical analysis and the simulation. The experimental results of the simulation and prototype show that the SIMO DC–DC converter with SMC-PID allowed to confirm in a clear way the validity and the feasibility of the proposed control strategy. An excellent control algorithm is particularly significant in the power system. We will pay more attention on the design of control algorithm in future work, and introduce the adaptive sliding-mode control algorithm, which endows the control system with better performance in the situation of startup and dynamic loads.

[1]M. Anun, M. Ordonez, I. G. Zurbriggen *et al.*, "Circular switching surface technique: High-performance constant power load stabilization for electric vehicle systems," IEEE Trans. Power Electron. **30**(8), 4560–4572 (2015).
[2]F. Gao, T. Yang, L. Zhang *et al.*, "An integrated electric vehicle power conversion system using modular multilevel converter," in *IEEE Energy Conversion Congress and Exposition (ECCE)* (IEEE, 2015), pp. 5044–5051.
[3]P. S. Mohanbhai and P. P. Mohanbhai, "Effective power and energy management for the dual source hybrid electric vehicle based on the measured drive cycle," in *IEEE 5th India International Conference on Power Electronics (IICPE)* (IEEE, 2012), pp. 1–6.
[4]R. J. Wai, L. S. Hong, and J. J. Liaw, "High-efficiency bidirectional single-input multiple-output power converter," IET Power Electron. **7**(5), 1278–1293 (2014).
[5]A. S. Patil and H. T. Jadhav, "A ZCS high efficient single input multiple output DC-DC converter with step up capability," in *International Conference on Electrical, Electronics, Signals, Communication and Optimization (EESCO)* (IEEE, 2015).
[6]E. Bonizzoni, F. Borghetti, P. Malcovati, F. Maloberti, and B. Niessen, "A 200 mA 93% peak efficiency single-inductor dual-output DC-DC buck converter," Analog Integr. Circuits Signal Process. **62**, 526–619 (2007).
[7]E. Bayer and G. Thiele, "A single-inductor multiple-output converter with peak current state-machine control," in *Twenty-First Annual IEEE Applied Power Electronics Conference and Exposition. APEC '06, 19–23 March 2006* (IEEE, 2006), p. 7.
[8]S.-C. Koon, Y.-H. Lam, and W.-H. Ki, "Integrated charge-control single-inductor dual-output step-up/step-down converter," in *IEEE International Symposium on Circuits and Systems May 2005* (IEEE, 2005), Vol. 4, pp. 3071–3074.
[9]M. W. May, M. R. May, and J. E. Willis, "A synchronous dual-output switching DC-DC converter using multibit noise-shaped switch control," in *IEEE International Solid-State Circuits Conference. Digest of Technical Papers* (IEEE, 2001), pp. 358–359.
[10]A. Pizzutelli and M. Ghioni, "Novel control technique for single inductor multiple output converters operating in CCM with reduced cross-regulation," in *Twenty-Third Annual IEEE Applied Power Electronics Conference and Exposition* (IEEE, 2008), pp. 1502–1507.

[11]M. Belloni, E. Bonizzoni, E. Kiseliovas, P. Malcovati, F. Maloberti, T. Peltola, and T. Teppo, "A 4-output single-inductor DC-DC buck converter with self-boosted switch drivers and 1.2 A total output current," in *IEEE International Solid-State Circuits Conference—Digest of Technical Papers* (IEEE, 2008), pp. 444–626.
[12]A. Sharma and Y. S. Pavan, "A single inductor multiple output converter with adaptive delta current mode control," in *IEEE International Symposium on Circuits and Systems* (IEEE, 2006), pp. 5643–5646.
[13]Y.-J. Woo, H.-P. Le, G.-H. Cho, G.-H. Cho, and S.-I. Kim, "Load-independent control of switching DC-DC converters with freewheeling current feedback," in *IEEE International Solid-State Circuits Conference—Digest of Technical Papers* (IEEE, 2008), pp. 446–626.
[14]P. Dai, S. Cauet, and P. Coirault, "Passivity-based control and sliding mode control of hybrid DC power source applied to hybrid electric vehicles," in *3rd International Conference on Systems and Control* (IEEE, 2013), pp. 691–696.
[15]R. Ling, M. Wu, Y. Dong, and Y. Chai, "High order sliding-mode control for uncertain nonlinear systems with relative degree three," Commun. Nonlinear Sci. Numer. Simul. **17**(8), 3406–3416 (2012).
[16]Y. He and F. L. Luo, "Sliding-mode control for DC-DC converters with constant switching frequency," IEE Proc.: Control Theory Appl. **153**(16), 37–45 (2006).
[17]J. Wang, S. Li, J. Fan *et al.*, "Nonlinear disturbance observer based sliding mode control for PWM-based DC-DC boost converter systems," in *The 27th Chinese Control and Decision Conference* (IEEE, 2015).
[18]S. Cauet, P. Coirault, and M. Njeh, "Diesel engine torque ripple reduction through LPV control in hybrid electric vehicle powertrain: Experimental results," J. Control Engineering Practice **21**(12), 1830–1840 (2013).
[19]Y. Wang, H. Xia, and Y. Cao, "Voltage controller of DC-DC buck converter using terminal sliding mode," in *IECON 2015—41st Annual Conference of the IEEE Industrial Electronics Society* (IEEE, 2015).
[20]S. Dwari, S. Jayawant, T. Beechner, S. K. Miller, A. Mathew, M. Chen, J. Riehl, and J. Sun, "Dynamics characterization of coupled-inductor boost DC-DC converters," in *IEEE Workshops on Computers in Power Electronics* (IEEE, Troy, NY, USA, 2006).
[21]P. Patra, A. Patra, and N. Misra, "A single-inductor multiple-output switcher with simultaneous buck, boost and inverted outputs," IEEE Trans. Power Electron. **27**(4), 1936–1951 (2012).
[22]Y. Chen, Y. Kang, S. Nie, and X. Pei, "The multiple-output DC–DC converter with shared ZCS lagging leg," IEEE Trans. Power Electron. **26**(8), 2278–2294 (2011).
[23]A. Nami, F. Zare, A. Ghosh, and F. Blaabjerg, "Multiple-output DC–DC converters based on diode-clamped converters configuration: Topology and control strategy," IET Power Electron. **3**(2), 197–208 (2010).
[24]C. Mullett and F. Cathell, "Improving the regulation of multi-output flyback converters," in *Twenty-Fourth Annual IEEE Applied Power Electronics Conference and Exposition* (IEEE, Palm Springs, USA, 2009), pp. 1923–1926.
[25]M. Huang and K. Chen, "Single-inductor multi-output (SIMO) DC-DC converters with high light-load efficiency and minimized cross-regulation for portable devices," IEEE J. Solid-State Circuits **44**(4), 1099–1111 (2009).
[26]H.-P. Le, C.-S. Chae, K.-C. Lee, S.-W. Wang, G.-H. Cho, and G.-H. Cho, "A single-inductor switching DC-DC converter with five output and ordered power-distributive control," IEEE J. Solid-State Circuits **42**(12), 2706–2714 (2007).
[27]S. Chong Tan, Y. M. Lai, and C. K. Tse, "General design issues of sliding-mode controllers in DC–DC converters," IEEE Trans. Ind. Electron. **55**(3), 1160 (2008).
[28]S. Oucheriah and L. Guo, "PWM-based adaptive sliding-mode control for boost DC–DC converters," IEEE Trans. Ind. Electron. **60**(8), 3291–3294 (2013).